The evolution of cloud and aerosol microphysics at the summit of Mt. Tai, China

Jiarong Li[1], Chao Zhu[1], Hui Chen[1,*], Defeng Zhao[1], Likun Xue[2], Xinfeng Wang[2], Hongyong Li[2], Pengfei Liu[3,4,5], Junfeng Liu[3,4,5], Chenglong Zhang[3,4,5], Yujing Mu[3,4,5], Wenjin Zhang[6], Luming Zhang[7], Kai Li[7], Min Liu[7], Hartmut Herrmann[1,2,8], Jianmin Chen[1,4,9,*]

[1]Shanghai Key Laboratory of Atmospheric Particle Pollution and Prevention (LAP3), Department of Environmental Science and Engineering, Institute of Atmospheric Sciences, Fudan University, Shanghai 200438, China

[2]Environment Research Institute, School of Environmental Science and Engineering, Shandong University, Ji'nan 250100, China

[3]Research Center for Eco-Environmental Science, Chinese Academy of Sciences, Beijing 10085, China

[4]Center for Excellence in Urban Atmospheric Environment, Institute of Urban Environment, Chinese Academy of Science, Xiamen 361021, China

[5]University of Chinese Academy of Sciences, Beijing 100049, China

[6]State Environmental Protection Key Laboratory of Urban Ambient Air Particulate Matter Pollution Prevention and Control, College of Environmental Science and Engineering, Nankai University, Tianjin 300071, China

[7]*Tai'an Municipal Ecological Environment Bureau, Shandong Tai'an Ecological Environment Monitoring Center, Tai'an 271000, China*

[8]Leibniz Institute for Tropospheric Research, Leipzig, Germany

[9]Shanghai Institute of Eco-Chongming (SIEC), No.3663 Northern Zhongshan Road, Shanghai 200062, China

Corresponding to: Jianmin Chen (jmchen@fudan.edu.cn) and Hui Chen (hui_chen@fudan.edu.cn)

Abstract. The influence of aerosols, both natural and anthropogenic, remains a major area of uncertainty when predicting the properties and behaviour of clouds and their influence on climate. In an attempt to understand better the microphysical properties of cloud droplets, simultaneous variations in aerosol microphysics and their potential interactions during cloud life cycles in the North China Plain, an intensive observation took place from 17 June to 30 July 2018 at the summit of Mt. Tai. Cloud microphysical parameters were monitored simultaneously with number concentrations of cloud condensation nuclei (N_{CCN}) at different supersaturations, $PM_{2.5}$ mass concentrations, particle size distributions and meteorological parameters. Number concentrations of cloud droplets (N_C), liquid water content (*LWC*) and effective radius of cloud droplets (r_{eff}) show large variations among 40 cloud events observed during the campaign. The low values of r_{eff} and *LWC* observed at Mt. Tai are comparable with urban fogs. Clouds in clean days are more susceptible to the change in concentrations of particle number (N_P), while clouds formed in polluted days might be more sensitive to meteorological parameters such as updraft velocity and cloud base height. Through studying the size distributions of aerosol particles and cloud droplets, particles larger than 150 nm played important roles on forming cloud droplets with the size of 5–10 μm. In general, *LWC* shows positive correlation with r_{eff}. As N_C increases, r_{eff} changes from a trimodal distribution to a unimodal distribution and shifts to smaller size mode. By assuming a constant cloud thickness, increase in N_C and decrease in r_{eff} would increase cloud albedo, which may induce a cooling effect on the local climate system. Our results contribute valuable information to enhance our understanding on cloud and aerosol

properties along with their potential interactions in North China plain.

1. Introduction

Clouds are key in the atmospheric hydrological cycle, which play an important role in the atmospheric energy budget and significantly influence the global and regional climate (Chang et al., 2019;Zhang et al., 2004b). Clouds can be physically described by their liquid water contents (*LWC*), number concentrations of droplets (N_C) and effective radius of droplets (r_{eff}). These parameters may show small inter-annual variations for the same monitoring station (Möller et al., 1996), but they vary over a large range for different cloud types (Quante, 2004), cloud altitudes (Padmakumari et al., 2017;Zhao et al., 2018) and in different parts of a cloud (Deng et al., 2009).

The interactions between the clouds and the aerosols are complex. Clouds efficiently remove aerosols by activating CCN to cloud droplets (Croft et al., 2010;Zhang et al., 2004a). The cloud processes can incorporate large amount of fine particulate mass (Heintzenberg et al., 1989), change the size distributions (Drewnick et al., 2007;Schroder et al., 2015) and alter the CCN compositions through homogeneous and heterogeneous reactions (Roth et al., 2016). In addition, the variation of aerosol number concentrations and size distributions could alter the cloud microphysics. Through studying microphysical characteristics of cloud droplet residuals at Mt. Åreskutan, Noone et al. (1990) found that larger cloud droplets preferred to form on larger Cloud Condensation Nuclei (CCN). The aerosol-cloud interaction has been investigated for cloud processes formed under both clean and polluted conditions. Padmakumari et al. (2017) found that convective clouds over land were characterized by lower *LWC* and higher N_C due to the increase of pollution aerosol. Ground-based observations by radiometers during the summers of the U.S. Studies in mid-Atlantic region revealed that cloud events with smaller droplets (< 7 μm) were more frequently observed in the polluted years than in the clean years (Li et al., 2017b). The influence of aerosols on the cloud microphysics is evident but varies for different regions and for different cloud types.

For a given liquid water content, aerosol particles can act as CCN, lead to higher number concentrations of cloud droplets with smaller sizes and result in higher albedo (Twomey effect or first indirect effect, FIE) (Twomey, 1974). Based on the principle of Twomey effect, calculations to evaluate the influence of aerosols on the cloud microphysics have been widely studied (Lohmann and Feichter, 2005;McComiskey et al., 2009;Twohy et al., 2005). However, arithmetic terms representing aerosol loading are different, such as using the number concentration of particles, the CCN concentration and the aerosol optical depth (AOD), which makes it difficult to compare the FIE from different studies. Positive relationships between aerosol loading and r_{eff}, called the "anti-Twomey effect", are widely observed, especially over land (Bulgin et al., 2008;Grandey and Stier, 2010;Tang et al., 2014;Wang et al., 2014).

The increase in the aerosol concentrations can result in a longer cloud lifetime, thus producing large cloud fractions (Koren et al., 2005;Albrecht, 1989), and increasing cloud top height and cloud thickness (Fan et al., 2013), which further

influence the regional and global climate (Rosenfeld, 2006;Seinfeld et al., 2016). The reduction in the precipitation or drizzle caused by the increase of aerosols (Andreae et al., 2004;Heikenfeld et al., 2019) delays the hydrological cycle (Rosenfeld, 2006). Through Model experiments with the Coupled Model Intercomparison Project phase 5 (CMIP5), Frey et al. (2017) found that the monthly mean cloud albedo of subtropical marine stratocumulus clouds increased with the addition of anthropogenic aerosols.

In situ measurements of cloud microphysics by aircraft or on high-altitude monitoring sites have provided some additional information for insight into the cloud processes (Allan et al., 2008;Li et al., 2017a;Padmakumari et al., 2017;Van Pinxteren et al., 2016;Reid et al., 1999). However, lacking knowledge of the size distributions of cloud droplets and aerosol particles makes it difficult to evaluate the cloud microphysics in small-scale regions (Fan et al., 2016;Khain et al., 2015;Sant et al., 2013). Discrepancy still exists between the widths of observed and simulated size distributions of cloud droplets (Grabowski and Wang, 2013). What's more, incompletely knowledge of the impact of cloud-aerosol interactions (Rosenfeld et al., 2014b), unresolved process of cloud formation (Stevens and Bony, 2013) and the lack of researches about the variation of cloud microphysical parameters at different cloud stages still hinder modelling studies.

The summit of Mt. Tai is the highest point in the centre of the North China Plain (NCP). Sufficient moisture in summer and dramatic temperature differences between day and night make it ideal for in situ orographic cloud monitoring (Li et al., 2017a). The summit of Mt. Tai is far away from anthropogenic emission sources on the ground. But high concentrations of inorganic ions in $PM_{2.5}$ (Zhou et al., 2009), abundant bacterial communities (Zhu et al., 2018), NH_3 and NO_x emissions form biomass burning (Chang et al., 2018) have been observed at the summit, thus a strong anthropogenic influence is existing. Previous studies of cloud samples collected at the same position showed high inorganic ion concentrations (Li et al., 2017a;Wang et al., 2011), which can be attributable to the increase of anthropogenic aerosol. In the study, in situ observations at the summit of Mt. Tai were presented to investigate the evolution of cloud microphysics coupled to simultaneous monitoring of aerosol size distributions, $PM_{2.5}$ mass and CCN concentrations within non-precipitating clouds. Two typical cloud processes are discussed in detail to elucidate the relationship of N_C, r_{eff} and LWC under clean or polluted conditions (indicated by N_P and N_{CCN}) and during the cloud life cycle. The present paper provides comprehensive information of cloud microphysical properties and their potential links to aerosol concentrations and size distribution. Implications of cloud and aerosol microphysics for cloud albedo and climate are discussed.

2. Experiments

2.1. Observation duration and site

From 17 June to 30 July 2018, 40 cloud events in total were monitored at the Shandong Taishan Meteorological Station at summit of Mt. Tai (Tai'an, China; 117°13' E, 36°18' N; 1545 m a.s.l.; Fig. S1). Mt. Tai is the highest point in the central of

North China Plain (NCP) and located within the transportation channel between the NCP and the Yangtze River Delta (Shen et al., 2019). The altitude of Mt. Tai is close to 1.6 km. This height is close to the top of the planetary boundary layer in Central East China and usually sited for the characteristic of particles inputting to clouds (Hudson, 2007). Orographic clouds, which are mainly formed in the boundary layer as air approaching the ridge, forced to rise up and cooled by adiabatic expansion (Choularton et al., 1997), frequently occur at the summit of Mt. Tai, especially in summer. Previous studies concentrated on cloud chemistry presented Mt. Tai is significantly influenced by anthropogenic emissions (Li et al., 2017a;Wang et al., 2011). In addition, fixed observation location are mainly applied to study the evolution of aerosol properties and cloud processing (Mertes et al., 2005;Roth et al., 2016). Thus, Mt. Tai is a good site for monitoring orographic clouds and simultaneously investigating aerosol and cloud microphysics. As shown in Fig. S2, the prevailing wind direction during this summer campaign is east wind (23.3%), southwest wind (22.8%) and south wind (21.9%), respectively. About 85.6% of wind speed was less than 8 m s^{-1}. While the monitored cloud events in the present study was mainly influence by south wind (34.7%) and southwest wind (22%). The arrangement of instruments was presented in Fig. S1(c).

2.2. Cloud microphysical parameters

A Fog Monitor (Model FM-120, Droplet Measurement Technologies Inc., USA), a forward-scattering optical spectrometer with sampling flow of 1 m^3 min^{-1}, was applied in situ for real-time displaying size distributions of cloud droplets and computing N_C, *LWC*, median volume diameter (*MVD*) and effective diameter (*ED*) in the size range of 2 to 50 μm (Spiegel et al., 2012). The corresponding equations are:

$$N_C = \Sigma N_i,$$

$$LWC = \frac{4\pi}{3}\Sigma N_i r_i^3 \rho_w,$$

$$MVD = 2 \times \left(\frac{\Sigma N_i r_i^3}{\Sigma N_i}\right)^{\frac{1}{3}}$$

$$ED = 2 \times r_{eff} = 2 \times \Sigma n_i r_i^3 / \Sigma n_i r_i^2,$$

Where N_i is the cloud number concentration at the ith bin, r_i represents the radius at the ith bin and ρ_w =1 g cm^{-3} stands for the density of liquid water. Droplets are categorized into manufacture's predefined 30 size bins with sampling resolution of 1 s. The size bin widths using this configuration were 1 μm for droplets < 15 μm and 2 μm for droplets > 15 μm. The true air speed calibration and size distribution calibration of FM-120 were carried out by the manufacturer using borosilicate glass microspheres of various sizes (5.0, 8.0, 15.0. 30.0, 40.0 and 50.0 μm, Duke Scientific Corporation, USA). The difference in optical properties between the glass beads and water was taken into account during the calibration process. In this study, the sampling inlet nozzle faced the main wind direction and was horizontally set. Cloud events are defined by the universally accepted threshold values in N_C and *LWC*, i.e., N_C > 10 # cm^{-3} and *LWC* > 0.001 g m^{-3} (Demoz et al., 1996). Too short cloud events with a duration < 15 minutes were excluded.

2.3. Aerosol size distribution

A Scanning Mobility Particle Sizer (SMPS, Model 3938, TSI Inc., USA) consisting of a Differential Mobility Analyzer (DMA, Model 3082, TSI Inc., USA) and a Condensation Particle Counter (CPC, Model 3775, TSI Inc., USA) was applied to monitor the size distributions of dehumidified aerosols through a PM_{10} inlet. The neutralized aerosols were classified by DMA to generate a monodisperse stream of known size according to their electrical mobility. The CPC placed downstream counts the particles and gives the number of particles with different sizes. In the present study, each scan was fixed at 5 min for every loop with a flow rate of 1.5 L min^{-1} sizing particles in the range of 13.6 - 763.5 nm in 110 size bins.

2.4. CCN number concentration

The N_{CCN} at certain supersaturations (SS) were quantified by a Cloud Condensation Nuclei Counter (Model CCN-100, DMT Inc., USA). The CCN counter was set at five SS values sequentially for 10 min each at 0.2 %, 0.4 %, 0.6 %, 0.8 % and 1.0 % with a full scan time resolution of 50 min. Data collected during the first 5 min of each SS was excluded since the CCN counter needs time for temperature stabilization after the change of SS. The ratio of sample flow to sheath flow was set at 1:10 with a total airflow of 500 ccm. The SS of CCN counter were calibrated before the campaign and checked at the end of the campaign with monodisperse ammonium sulfate particles of different sizes (Rose et al., 2008).

2.5. $PM_{2.5}$ concentrations and meteorological parameters

The $PM_{2.5}$ mass concentration was measured using a beta attenuation and optical analyzer (SHARP monitor, model 5030i, Thermo Scientific Inc., USA). Meteorological parameters including the ambient temperature (T_a, ℃), relative humidity (RH), wind speed (WS, m s^{-1}) and wind direction (WD, °) were provided by Shandong Taishan Meteorological Station at the same observation point. The ground-level temperature (T_g), ground-level pressure (P_g), and dew point temperature (T_{gd}) were supported by National Meteorological Observatory – Tai'an Station (station number: 54827, 117°9' E, 36°9' N, 128.6 m a.s.l) (Fig. S1(a)), which sited in the south plain of Mt. Tai.

2.6. Calculation of cloud base height

In the present study, the estimated lifting condensation level (LCL) is applied to represent the cloud base height (CBH) due to the lack of corresponding instruments. The calculation of LCL depends on the meteorological parameters measured at Tai'an Station. The ground-level data of temperature, dew point temperature, and pressure were used as input parameters (Georgakakos and Bras, 1984):

$$p_{LCL} = \frac{1}{(\frac{T_g - T_{gd}}{223.15} + 1)^{3.5}} \times p_g$$

$$T_{LCL} = \frac{1}{(\frac{T_g - T_{gd}}{223.15} + 1)} \times T_g$$

$$CBH = 18400 \times (1 + \frac{T_{LCL} - T_g}{273}) \times \lg \frac{p_g}{p_{LCL}}$$

Where p_{LCL} is the *LCL* pressure; T_{LCL} is the *LCL* temperature.

During the observation period, *CBH* ranged from 460.3 m to 3639.1 m with the average value of 1382.5 m. As shown in Fig. 2(b), the observation station would be totally enveloped in clouds and around when cloud events occurred. The corresponding distance between the observation point and *CBH* was represented in Fig. 2(b)

2.7. Calculation of *AIE*

Aerosol indirect effect (AIE), which represents simply approximations of the derivatives of the cloud microphysics (r_{eff} and N_C) with respect to changes in aerosol concentrations (McComiskey et al., 2009;Feingold et al., 2001), is applied to study the influence of N_P on cloud microphysics and calculated as:

$$AIE_r = -\left(\frac{\Delta ln r_{eff}}{\Delta ln N_P}\right)_{LWC}, 0< AIE_r <0.33$$

$$AIE_N = -(\frac{\Delta ln N_C}{\Delta ln N_P}), 0< AIE_N <1$$

Where N_P is applied as an proxy of aerosol amount (Zhao et al., 2012;Zhao et al., 2018).

2.8. Calculation of cloud albedo

Cloud albedos can be calculated using the equations shown below (Seinfeld and Pandis, 2006). Assuming the cloud droplet size distribution can be approximated as monodisperse and the cloud is vertically uniform with respect to droplet size distribution (Stephens, 1978), the cloud optical thickness (τ_c) could be obtained by

$$\tau_c = h(\frac{9\pi LWC^2 N_c}{2\rho_w^2})^{\frac{1}{3}}$$

Where h is the thickness of the cloud and ρ_w is the density of cloud water.

For the nonabsorbing and horizontally homogeneous cloud, the two-stream approximation for the cloud albedo (R_c) gives as (Lacis and Hansen, 1974)

$$Albedo = \frac{\sqrt{3}(1-g)\tau_c}{2 + \sqrt{3}(1-g)\tau_c}$$

Where g is the asymmetry factor. The radius of cloud droplets was much greater than the wavelength of visible light, hence g is 0.85. The equation before becomes to

$$Albedo = \frac{\tau_c}{\tau_c + 7.7}$$

3. Results and discussion

3.1. Overview of the cloud microphysics

During 17th June to 30th July 2018, 40 cloud events were captured at the summit of Mt. Tai. Large ranges of cloud microphysics have been observed during the campaign. The averaged N_C, *LWC*, and r_{eff} of the 40 cloud events at the summit of Mt. Tai varied over the ranges of 59–1519 # cm^{-3}, 0.01–0.59 g m^{-3} and 2.6–7.4 μm, respectively (Table S1). The monitored number concentration of cloud droplets at Mt. Tai both in the present study and in 2014 can reach 2000-3000 # cm^{-3} (Li et al., 2017a), which is much higher than those values (with a range of 10–700 # cm^{-3}) for city fogs and convective and orographic clouds (Allan et al., 2008;Li et al., 2011;Padmakumari et al., 2017) (Table 1). It represented clouds at Mt. Tai were characterized with high N_C.

The microphysics of different clouds and fogs can generally be distinguished in a plot of r_{eff} (or *MVD*) against *LWC*. As illustrated in Fig. 1, the *LWC* increases as the altitude increases generally in order of city fogs, orographic clouds and convective clouds, and Mt. Tai generally according the rule. It is consistent with the study by Penner et al. (2004) that *LWC* within clouds increases linearly with altitude. For *LWC* values of clouds at Mt. Tai, we monitored the high values, which are comparable with convective clouds, and the low values, which are similar to city fogs (Fig. 1). It indicated that clouds at Mt. Tai appeared to show a larger range of *LWC* values. The increase of *LWC* at Mt. Tai should be determined by the increase of r_{eff} and/or N_C. But sometimes only one factor plays the determining role. As illustrated in Table S1, N_C r_{eff} and LWC in cloud event 20 (CE-20) were 1519 # cm^{-3}, 5.2 μm and 0.54 g m^{-3}, respectively, while the corresponding values in CE-16 were 59 # cm^{-3}, 9.8 μm and 0.14 g m^{-3}, respectively. Even though r_{eff} of CE-20 was smaller compared with CE-16, but the higher N_C determined the larger *LWC* of clouds in CE-20. In the following parts, the evolution of cloud and aerosol microphysical properties were presented. The influence of meteorological parameters (such as updraft velocity and cloud base height) and aerosol particle on cloud microphysics were discussed.

3.2. Analysis on typical cloud processes

By assuming a density of ρ = 1.58 g cm^{-3} (Cross et al., 2007), the mass concentrations of particles, which were calculated from the aerosol number size distribution measured by SMPS and named as $PM_{0.8}$, was highly consistent with $PM_{2.5}$, especially when $PM_{2.5}$ was less than 20 μg m^{-3} (Fig. 2(c)). Based on the mass concentration ($PM_{2.5}$) and the number concentration (N_P, which represented the total number concentration of aerosol particles measured by SMPS) of aerosols, two typical cloud processes were selected and analysed with their special characteristics. The influence of topography and updraft velocity (v_{up}) on the measurement of Fog Monitor could be ignored during the two cloud processes (Supplement). In cloud process-1 (CP-1, including one cloud event – CE-19), cloud droplets formed under a relatively stable (wind speed < 4 m s^{-1}) and clean ($PM_{2.5}$ ≈ 10.9 μg m^{-3}, N_P ≈ 1425 # cm^{-3}) conditions accompanied by a slow increase of T_a (Fig. 2 and Fig. 3). During daytime,

especially in the afternoon, the $PM_{2.5}$ mass concentration dramatically increased with few changes in wind speed and wind direction, meanwhile N_P reached to about 5000 # cm^{-3} (Fig. 3). CP-1 persisted for 74 h, making it the longest cloud event during the present campaign. Quite different from CP-1, cloud process-2 (CP-2) contained eight cloud events (CE-20 to CE-26, Fig. 3) and occurred periodically under high $PM_{2.5}$ (Fig. 2, 50.7 μg m^{-3} in average) as well as high N_P (Fig. 3, 1694 # cm^{-3} in average) conditions. Cloud events in CP-2 formed after sunset with sharp decreasing of $PM_{2.5}$ and N_P, and transitorily dissipated at noon accompanied with the increase of $PM_{2.5}$, N_P, T_a and cloud base height (*CBH*). For cloud water samples collected during CP-1 and CP-2, the percentage of chemical compositions did not change a lot (Fig. S5). Three dominant main anions (sulfate, nitrate and ammonia) accounted for 93.39% in CP-1 and 90.37% in CP-2 of the total measured ions. The high concentration of secondary ions in the cloud water samples indicated that clouds at Mt. Tai were dramatically influenced by anthropogenic emissions.

CP-1 was separated into four stages, including SL1 (stage-low 1), SH1 (stage-high 1), SL2 (stage- low 2), and SH2 (stage-high 2) based on the aerosol concentrations (Fig. 3(a)). The characteristics of SL1 and SL2 were low N_C (383 and 347 # cm^{-3}, respectively), large r_{eff} (7.26 and 6.36 μm, respectively) and high LWC/N_C (1.01 and 0.75 ng $\#^{-1}$, respectively, which represents averaged water each cloud droplet contained) (Fig. 3(b)). During SH1 and SH2, dramatic increase of N_C (to 949 and 847 # cm^{-3}, respectively) and decrease of r_{eff} (to 4.90 and 4.88 μm, respectively) and LWC/N_C (to 0.35 and 0.36 ng $\#^{-1}$, respectively) occurred with the increase of N_P (to 4196 and 4665 # cm^{-3}, respectively).

Each cloud event of CP-2 was separated into activation stage (S1), collision-coalescence stage (S2), stable stage (S3), and dissipation stage (S4) according to the regular changes of N_C and LWC/N_C (Fig. 3(a)). In S1, N_C dramatically increased to its maximum value among the cloud events. In S2, N_C declined sharply to a stable value, meanwhile LWC/N_C reached the maximum value. In S3, N_C was stable or slightly varied and LWC/N_C started to decrease. In S4, both N_C and LWC/N_C decreased sharply again and finally arrived zero. Even though the two stages (S2 and S3) in CE-25 were not totally follow the division rules, the other six cloud events followed well. It indicated that the division was helpful to study the variations of cloud microphysical properties during CP-2. The newly formed cloud droplets during S1 were characterized by small size, high N_C and low LWC/N_C values (Fig. 2(f) and 3(b)). For example, about 2310 # cm^{-3} of cloud droplets can quickly form in the first 2 hours of CE-20. The r_{eff} of these droplets was smaller than 4.1 μm and LWC/N_C was about 0.2 ng $\#^{-1}$. In going from S2 to S3, the strong collision-coalescence between cloud droplets caused the increase of both r_{eff} and LWC/N_C. In S4, the increase of $PM_{2.5}$, through evaporation of cloud droplets or lifting of *CBH* (Fig. 2), would cause the vanishment of cloud events (Mazoyer et al., 2019;Li et al., 2017a).

3.2.1. Relationships among N_P, N_{CCN} and N_C

In the present study, both positive and negative relations between N_P and N_C were observed. N_P and N_C showed consistent variation in CP-1. But in CP-2, an obviously inverse relation was found between N_P and N_C in S1 and S4, while a

simultaneously variation was found between N_P and N_C in S2 and S3 (Fig. 3(a), Fig. 4(b), and Fig. 4(c)). Some in situ observations (Lu et al., 2007;Mazoyer et al., 2019) and modelling studies (Heikenfeld et al., 2019;Zhang et al., 2014) supported the viewpoint that the increase of N_P brings more CCN and further increases N_C, which caused the positive relation between N_P and N_C. In contrast, some recent studies of fogs also suggested that the increase of N_P would decrease the ambient supersaturation and then decrease N_C (Boutle et al., 2018;Mazoyer et al., 2019). Besides, Modini et al. (2015) found negative relation between N_C and the number of particles with diameters larger than 100 nm due to the reduction of supersaturation by coarse primary marine aerosol particles. In general, the relation between *Np* and *Nc* could be affected by many factors, including competition of water vapor between aerosol particles and/or cloud droplets, the scavenging of particles by cloud droplets, and new particles formation through cloud processes. In the present study, we found *LWC/Nc* should play an important role on the relation between N_P and N_C. The averaged *LWC/Nc* was 0.61 ng $\#^{-1}$ in CP-1 and were 0.15, 0.42, 0.39, 0.16 ng $\#^{-1}$ in S1, S2, S3, S4, respectively, in CP-2. High LWC/N_C value indicating water was sufficient for new cloud droplet formation. Once N_P increased, part of the cloud water was taken away by the CCN in the particles to form new droplets, and the remaining amount of water was still sufficient to maintain the previous droplets in liquid state. Positive relationship was existed between N_P and N_C. However, lower LWC/N_C values, to some extent, limited the formation of new cloud droplets. The activated particles grew at the beginning of the cloud cycle would lower the surrounding supersaturation and to some extent limit further aerosol activation (Ekman et al., 2011). The part of water taken by the CCN in the particles was not enough to active all of them to be new droplets and the remaining amount of water was also insufficient to maintain all the previous droplets in liquid state. Then the N_C would decrease and the more the N_P, the sharper decrease the N_C. Thus, the inverse relationship would be observed.

The ratio between N_{CCN} and N_P could reflect the activation ratio of aerosol particles. As shown in Fig. S6, N_{CCN} increased with the increase of *SS*. In addition, N_{CCN} of CP-2 was higher than that of CP-1 at the same *SS*. In order to compare with previous studies as discussed below, *SS* = 0.2 % was chosen to calculate N_{CCN}/N_P, which represented the activation ratio of aerosol particles. As shown in Fig. 3(b), $N_{CCN,0.2}/N_p$ (activation ratio at a certain SS = 0.2 %) ranged from 0.06 to 0.69 in CP-1 yet it was range from 0.22 to 0.66 in CP-2. The averaged value of 0.30 in CP-1 was smaller than that of 0.38 in CP-2 and values lower than 0.22 did not appear during CP-2. It indicated that the activation of aerosol particles in CP-2 was relatively easier. Both the size distribution and the chemical composition could impact the cloud-nucleating ability of aerosol particles (Dusek et al., 2006;Mazoyer et al., 2019). In order to discuss the activation ratio with aerosol size, Fig. S7 showed the relation between $N_{CCN,\,0.2}/N_P$ with GMr_P during CP-1 and CP-2. As can be seen, the higher correlation of $N_{CCN,\,0.2}/N_P$ with GMr_P during CP-1 represented that the activation of aerosols during CP-1 was mainly influenced by physical properties compared with CP-2. Besides, Asmi et al. (2012) found that higher N_{CCN}/N_P and more concentrated plot of N_{CCN} versus N_P were usually occurred during winter when higher fraction of aged organics was observed during the observation program at Puy-de-Dome, France. In this study, the plot of $N_{CCN,0.2}$ versus N_P was more scatter in CP-1 than that in CP-2 (Fig. S8). Even though the settled *SS* in

the present study (*SS* = 0.2%) is different from that at puy-de-Dome (*SS* = 0.24%), most of the data points of CP-1 and CP-2 were distributed between the two recommended dashed lines (the visually defined boundaries in within most of the data are centered, Fig. S8) by Asmi et al. (2012). It suggested that the difference of aerosol organic chemical compositions during CP-1 and CP-2 might also a reason for explaining the different activation ratio of aerosol particles during these two cloud processes.

3.2.2. Aerosol Indirect Effect on Cloud Microphysics

According to the studies of AIE_r and AIE_N of CP-1 and CP-2, it was indicated that cloud droplets numbers are more sensitive to N_P under smaller aerosol amount conditions. The calculation of AIE_r was shown in Fig. S9 and summarized in Fig. 4. As shown in Fig. 4(a), except for the out-of-bound AIE_r values calculated with insufficient data points when *LWC* was larger than 0.7 g m^{-3}, AIE_r of 0.181–0.269 for CP-1 were always higher than those of 0.025–0.123 for CP-2 in corresponding narrow *LWC* ranges. We verified this with AIE_N. Due to the limitation of the Fog Monitor, the number of cloud droplets may be underestimated during the activation and dissipation stages (Mazoyer et al., 2019), which caused the low R^2 of CP-1. In CP-2, only the data of S2 and S3 were employed to calculate AIE_N for excluding the points in S1 and S4, which may be underestimation. As shown in Fig. 4(b) and Fig. 4 (c) both the slope (0.144) and R^2 (0.050) of CP-2 are lower than those (0.544 and 0.282, respectively) of CP-1. It verified that cloud droplets in CP-2 were little influenced by aerosols. In the previous studies, both observation and modelling studies also found that AIE_r was higher under smaller aerosol amount conditions. Twohy et al. (2005) measured the equivalent AIE_r of 0.27 in the California coast while Zhao et al. (2018) used satellite observations to attribute lower values of 0.10-0.19 for convective clouds over Hebei, one polluted region in China. Using an adiabatic cloud parcel model, Feingold (2003) found that AIE_r increased from 0.199 to 0.301 when N_P decreased to less than 1000 # cm^{-3}. By using the Community Atmospheric Model version 5 (CAM5), Zhao et al. (2012) also found high AIE_r values in the tropical West Pacific at Darwin (TWP) due to the low N_P in December, January, and February. In addition, the increase of aerosol concentrations would cause stronger albedo enhancements when pollution is low in the ambient air (Platnick et al., 2000). Through studying the impact of ship-produced aerosols on the microstructure and albedo of warm marine stratocumulus clouds, Durkee et al. (2000) found that the clean and shallow boundary layers would be more readily perturbed by the addition of ship particle effluents. What's more, the meteorological conditions and the topography during the monitoring period would also affect the microphysical properties of clouds. The sensitivity analysis of N_C to *CBH* and v_{up} was estimated by applying the equation as $S(X_i)=\partial \ln N_C/\partial \ln X_i$, where X_i represented *CBH* and v_{up}. As shown in Talbe S2, CP-2 was more sensitive to the variation of meteorological parameters if compared with CP-1. It was consistent with the study of McFiggans et al. (2006). They found that the sensitivity of N_C to v_{up} increased while the sensitivity of N_C to N_P decreased when N_P > 1000 # cm^{-3}. In the present study, the higher values of AIE_r and AIE_N of CP-1 indicated that if the same amount of aerosol particles entered the cloud, the size of cloud droplets in CP-1 would decrease more than that in CP-2. The albedo during CP-1 would be more susceptible to the change of aerosol particles. While the higher values of S(*CBH*) and S(v_{up}) of CP-2 indicated that CP-2 was

more sensitive to the change of *CBH* and v_{up}. It might cause the periodical variations of cloud microphysical properties during CP-2.

The positive AIE_r and AIE_N at Mt. Tai mean that the increase in N_P are accompanied by decreased r_{eff} and increased N_C. No negative AIE_r were found in the present study. Yuan et al. (2008) and Tang et al. (2014) applied AOD to represent aerosol loading and found negative AIE_r (indicating r_{eff} increased with the increasing of AOD) near coastlines of the Gulf of Mexico, the South China Sea and over Eastern China with the surrounding sea. By using the 2-D Goddard Cumulus Ensemble model (GCE), Yuan et al. (2008) explained that the positive relationship between r_{eff} and AOD appeared to originate from the increasing slightly soluble organics (SSO) particles. The increase of SSO would act to increase of the critical supersaturation for particles to be activated and resulted in less numbers of activated particles. With Moderate Resolution Imaging Spectroradiometer (MODIS) observations, Tang et al. (2014) explained that the negative *AIE* values were likely attributable to meteorological conditions from the South and Southeast China, which usually favoured transport of both pollutants and water vapour and led to simultaneous increases in both AOD and r_{eff}. Compared with these regions, the summit of Mt. Tai is relatively far from the sea (around 230 km from the Bohai Sea and Yellow Sea) (Guo et al., 2012). The air brought aerosols but with less moist. It might hinder the growth of cloud droplets and caused the negative relation between N_P and r_{eff}. An increase in *LWC* might reduce the *AIE*, especially at coastal sites (McComiskey et al., 2009;Zhao et al., 2012). However, weak variations of AIE_r with an increase of *LWC* were found at Mt. Tai (Fig. 4(a)). It may be due to the high aerosol loading during cloud processes (Zhao et al., 2012).

3.2.3. Size distribution of cloud droplets and particles

To illustrate the evolution of the aerosol particles and the cloud droplets during the cloud processes, the size distributions of N_P and N_C during different cloud stages are plotted in Fig. 5. For each of the four size bins ranged from 2 to 13 μm, cloud number concentrations of SL1 and SL2 were lower than those of SH1 and SH2. In the size bin of 13–50 μm, however, N_C of SL1 and SL2 were the largest (Fig. 5(b)). This size distributions of cloud droplets in SL1 and SL2 resulted in the larger r_{eff} during the two stages, which was consistent with the result shown in Fig. 3(b). During SH1 and SH2 in CP-1, the numbers of aerosol particles in all size bins increased. But the increase of aerosol particles larger than 150 nm was the smallest, indicating that aerosols larger than 150 nm were more easily activated into cloud droplets. The activation of aerosol particles with the size larger than 150 nm in the present study dramatically increased N_C of 5–10 μm and made N_C of SH1 and SH2 in different size bins all comparable with those of CP-2 (Fig. 5(b)).

As shown in Fig. 5(c), cloud droplets with D_C ranging from 5 to 10 μm had high N_C in each stage in CP-2 and cloud droplets with D_C ranging from 13 to 50 μm had low N_C in each stage if compared to CP-1. It caused the lower r_{eff} in CP-2 than CP-1. During CP-2, aerosol particles with diameters larger than 150 nm quickly decreased by activation when cloud events occurred, while the number of aerosol particles in the size of 50-150 nm were slightly influenced by cloud events (the first

panel of Fig. 5(a). It was consistent with the study of Targino et al. (2007) who found aerosol size distributions of cloud residuals, which represented aerosol particles activated to cloud droplets, peaked at about 0.15 μm at Mt. Åreskutan. Mertes et al. (2005) also found that particles centered at d_p = 200 nm could be efficiently activated to droplets while most Aitken mode particles remained in the interstitial phase. Compared with other stages, S1 had the highest N_C in three size bins of [2, 5) μm and [5, 7) μm. It indicated that large numbers of cloud droplets with small sizes were formed in the beginning of cloud events in CP-2.

3.3. Relations among *LWC*, r_{eff} and N_C

The 5 min averaged *LWC* for CP-1 and CP-2 is plotted against corresponding r_{eff} in Fig. 6(a). Large cloud droplets (r_{eff} > 8 μm) were observed in CP-1, while the r_{eff} for CP-2 varied narrowly in the range of 2.5–8 μm.

Cloud droplets with r_{eff} > 8 μm only occurred in the two relatively clean stages, SL1 and SL2, during CP-1. It was due to the weaker competition among droplets at lower N_{CCN} conditions. This has also been observed in the U.S. Mid-Atlantic region where cloud droplets with larger sizes are more easily formed with lower N_{CCN} (Li et al., 2017b). At the same *LWC* level, the growth of cloud droplets during SH1 and SH2 was obviously limited if compared with SL1 and SL2, which is referred to as the "Twomey effect" (Twomey, 1977). This is consistent with the illustration in Fig. 3 that cloud droplets in SH1 and SH2 were smaller.

The variation r_{eff} and/or N_C can influence *LWC*, while the key factor may be different in different stages of the cloud. As shown in the lower panel of Fig. 6(a), CE-20 was taken as an example to discuss the relation among *LWC*, r_{eff} and N_C in different cloud stages. During S1, the existing numerous CCN (Fig. 3(a)) were quickly activated to form cloud droplets. The newly formed droplets are characterized with small sizes but large numbers. They will suppress the beginning of collision-coalescence processes (Rosenfeld et al., 2014a) and may further significantly delay raindrop formation Qian et al. (2009). In S1, positive relation existed between N_C and r_{eff}. Both the increase in N_C (from 1188 # cm^{-3} to 2940 # cm^{-3}) and the growth of r_{eff} (from ~3.5 μm to ~4.5 μm) boosted the *LWC* in this stage. This is different from Mazoyer et al. (2019)'s result that they found a clearly inverse relationship between the number and the size of droplets at the beginning of the first hour of fog events during the observation in suburban Paris. When compared with fog, cloud is usually formed under conditions with more condensible water vapour (Fig. 1). The limited growth of droplets in fog will not occur in cloud. It caused the positive relationship with cloud droplet number and droplet size. At the beginning of S2, N_C reaches the maximum. The high N_C yields a great coalescence rate between cloud droplets. Meanwhile, the coalescence process is self-accelerating (Freud and Rosenfeld, 2012) and thus causes the quick decrease of N_C (Fig. 3(a)). This makes cloud droplets in S2 characterized by larger sizes as well as lower number concentrations, whilst *LWC* simply varies in a relatively narrow range (Fig. 6(a)). During S3, N_C is almost constant due to the formation, coagulation, and evaporation of the cloud droplets reaching a balance. As shown in the panel, the relationship between r_{eff} and *LWC* in this stage could be fitting as $r_{eff} = a \times LWC^{0.34 \pm 0.02}$, which means under the

increase of *LWC*, the N_C was almost unchanged. The variation of *LWC* values is mainly due to the changes of droplet sizes. At the dissipation stage of S4, the increase of *CBH* brought air with low *RH* and high N_P to the summit of Mt. Tai and caused the dissipation of cloud events (Fig. 2(c) and Fig. 3(a)). The previously activated CCN returned back to the interstitial aerosol phase due to the evaporation of the droplets (Verheggen et al., 2007). Both N_C and r_{eff} decline. It also illustrates in Fig. 5(c) that all the N_C of the five size bins of cloud droplets decrease in S4.

In order to investigate the variation of r_{eff} upon N_C, the distribution of r_{eff} was classified with different N_C ranges in Fig. 6(b). For N_C < 1000 # cm^{-3}, r_{eff} displayed a trimodal distribution and concentrated on 3.25 μm (Peak-1), 4.86 μm (Peak-2) and 7.52 μm (Peak-3), respectively. Peak-1 corresponded to cloud droplets with low N_C, *LWC*, and r_{eff} values while the $N_{CCN0.2}$ was very high (Fig. 6(c)). These points represented cloud droplets in the incipient stage or the dissipation stage of cloud events where large numbers of CCN exist in the atmosphere. Peak-2 and Peak-3 represented the mature stages for cloud events with different environmental conditions. Peak-3 represented cloud droplets formed under a relatively cleaner atmosphere. In this circumstance, CCN were efficiently activated and had a lower concentration remaining in the atmosphere (Fig. 6(c)). The sufficient ambient water vapour accelerated the growth of the formed droplets, which were characterized with low N_C and *LWC* but large r_{eff}. Peak-2 represented cloud droplets formed under relatively polluted conditions and was the only peak found for N_C larger than 1000 # cm^{-3}. With the increase of N_C, the distribution of this peak narrowed and slightly moved to lower r_{eff} mode.

The thickness of orographic cloud was easily influenced by the specific topography and environmental conditions (Barros and Lettenmaier, 1994;Welch et al., 2008). If assuming the cloud thickness during CP-1 and CP-2 were equal, albedo would depend on the values of *LWC* and N_C as described in Section 2.8. Cloud albedo during CP-2 was always higher than that during CP-1, especially when the cloud thickness was lower than about 2500 m (Fig. 6(d)). Through studying marine stratocumulus clouds in the north-eastern Pacific Ocean, Twohy et al. (2005) also found that the increase of N_C by a factor of 2.8 would lead to 40% increase of albedo going from 0.325 to 0.458. It indicated that the higher N_C would increase the cloud albedo if assuming no change of cloud thickness.

4. Conclusion

From 17th June to 30th July 2018 in-situ observations of number concentrations and size distributions of aerosol particles and cloud droplets are employed to show aerosol-cloud interactions at the summit of Mt. Tai. Large variations of the characteristic values in terms of N_C, *LWC* and r_{eff} were found during the observation period. Cloud droplets with smaller r_{eff} and lower *LWC* exist at Mt. Tai, which are similar to urban fogs.

Two typical cloud processes, CP-1 and CP-2, are applied to study the cloud-aerosol interactions based on the aerosol characteristics (especially N_P and N_{CCN}) before cloud onsets. For the CP-1, which corresponded to relatively clean conditions,

water content is sufficient while N_{CCN} limits cloud droplet formation. The newly formed cloud droplets are characterized with low N_C but high LWC/N_C and large r_{eff}. With the increase of aerosol concentration, N_C dramatically increased by about three times. Large numbers of N_{CCN} will compete for the system water content with the formed cloud droplets and, as a result, further dramatically decrease the LWC/N_C and r_{eff} values of cloud droplets. In CP-2, N_P before the cloud onset is high and N_{CCN} is sufficient. Water vapour becomes the limitation for cloud formation. Large numbers of small cloud droplets with low LWC/N_C formed in the incipient stage of cloud events. In addition, periodically changes of cloud microphysical properties were found. Both positive and negative relations between N_P and N_C have been observed in the present study, which depended on the values of LWC/N_C.

Both positive AIE_r and AIE_N values at Mt. Tai indicate that the increase of N_P will decrease r_{eff} and increase N_C of cloud droplets. AIE_r and AIE_N values are lower with higher N_P and N_{CCN}. This represents that the increase of N_P will more strongly decrease the size and increase the number of cloud droplets under the conditions of smaller aerosol amount. Through studying the size distributions of aerosol particles and cloud droplets, higher N_C in the size bin of 13–50 μm resulted in the larger r_{eff} during the two clean stages in CP-1. Particles larger than 150 nm can be efficiently activated to cloud droplets and make important contributions to the increase of cloud droplets in the size range of 5–10 μm.

The LWC of cloud depended on the change of r_{eff} and N_C. However, the decisive factor may differ at different stages of the cloud. In general, the r_{eff} of cloud droplets correlates positively with LWC. But in different N_C ranges, the r_{eff} of cloud droplets show different distribution shapes. For $N_C < 1000$ # cm^{-3}, r_{eff} displayed a trimodal distribution. Three peaks were 3.25, 4.86 and 7.52 μm, respectively. With the increase of N_C, a narrowed unimodal distribution of r_{eff} appeared and the peak value slightly moved towards lower r_{eff} mode. For a constant cloud thickness, the increased N_C and decreased r_{eff} dramatically increase the cloud albedo, which may further influence the regional climate in the North China Plain.

The local topography of the surrounding areas at Mt. Tai supplies a potential access for aerosol transportation and can affect the measured cloud droplet distributions by increasing turbulence or causing orographic flows. Even though the summit of Mt. Tai is far away from the polluted sources, the transported CCN could change the cloud microphysical properties (i.e., during CP-1). The cloud microphysical parameters derived in our study characterized the cloud features in the North China Plain, and provided valuable data for modelling studies of cloud microphysics in the future.

Data availability

All data used to support the conclusion are presented in this paper. Additional data are available upon request. Please contact the corresponding authors (Jianmin Chen (jmchen@fudan.edu.cn) and Hui Chen (hui_chen@fudan.edu.cn)).

Author contribution.

JC, HC conceived the study. JL and CZ performed the field experiments and sampled cloud water. JL analysed the data

and wrote the main manuscript text. JC, HC, DZ, CZ and HH revised the initial manuscript. LX, XW and HL supported the meteorological data and $PM_{2.5}$ mass concentration. PL, JL, CZ, YM and WZ assisted in instrument maintenance. LZ, KL and ML contributed to the organization and arrangement of the field observation. LZ provided the meteorological parameters of Tai'an City. All of the authors discussed the results, and contributed to the final manuscript.

Competing interests.

The authors declare no conflict of interest.

Acknowledgement

This work was supported by the Ministry of Science and Technology of China (2016YFC0202700), Tai'an Research Project (SDTASJ2018-0761-00), National Natural Science Foundation of China (91843301，91743202, 41805091, 21806020), and Marie Skłodowska-Curie Actions (690958-MARSU-RISE-2015).

References

Albrecht, B. A.: Aerosols, cloud microphysics, and fractional cloudiness, Science, 245, 1227-1230, 10.1126/science.245.4923.1227, 1989.

Allan, J. D., Baumgardner, D., Raga, G. B., Mayol-Bracero, O. L., Morales-Garcia, F., Garcia-Garcia, F., Montero-Martinez, G., Borrmann, S., Schneider, J., Mertes, S., Walter, S., Gysel, M., Dusek, U., Frank, G. P., and Kraemer, M.: Clouds and aerosols in Puerto Rico - a new evaluation, Atmos. Chem. Phys., 8, 1293-1309, 10.5194/acp-8-1293-2008, 2008.

Andreae, M. O., Rosenfeld, D., Artaxo, P., Costa, A. A., Frank, G. P., Longo, K. M., and Silva-Dias, M. A. F.: Smoking rain clouds over the Amazon, Science, 303, 1337-1342, 10.1126/science.1092779, 2004.

Barros, A. P., and Lettenmaier, D. P.: DYNAMIC MODELING OF OROGRAPHICALLY INDUCED PRECIPITATION, Reviews of Geophysics, 32, 265-284, 10.1029/94rg00625, 1994.

Boutle, I., Price, J., Kudzotsa, I., Kokkola, H., and Romakkaniemi, S.: Aerosol-fog interaction and the transition to well-mixed radiation fog, Atmos. Chem. Phys., 18, 7827-7840, 10.5194/acp-18-7827-2018, 2018.

Bulgin, C. E., Palmer, P. I., Thomas, G. E., Arnold, C. P. G., Campmany, E., Carboni, E., Grainger, R. G., Poulsen, C., Siddans, R., and Lawrence, B. N.: Regional and seasonal variations of the Twomey indirect effect as observed by the ATSR-2 satellite instrument, Geophys. Res. Lett., 35, 10.1029/2007gl031394, 2008.

Chang, Y., Zhang, Y., Li, J., Tian, C., Song, L., Zhai, X., Zhang, W., Huang, T., Lin, Y. C., Zhu, C., Fang, Y., Lehmann, M. F., and Chen, J.: Isotopic Constraints on the Atmospheric Sources and Formation of Nitrogenous Species in Biomass-Burning-Influenced Clouds, Atmos. Chem. Phys. Discuss., 2018, 1-27, 10.5194/acp-2018-1196, 2018.

Chang, Y., Guo, X., Tang, J., and Lu, G.: Aircraft measurement campaign on summer cloud microphysical properties over the Tibetan Plateau, Sci. Rep., 9, 10.1038/s41598-019-41514-5, 2019.

Choularton, T. W., Colvile, R. N., Bower, K. N., Gallagher, M. W., Wells, M., Beswick, K. M., Arends, B. G., Mols, J. J., Kos, G. P. A., Fuzzi, S., Lind, J. A., Orsi, G., Facchini, M. C., Laj, P., Gieray, R., Wieser, P., Engelhardt, T., Berner, A., Kruisz, C., Moller, D., Acker, K., Wieprecht, W., Luttke, J., Levsen, K., Bizjak, M., Hansson, H. C., Cederfelt, S. I., Frank, G., Mentes, B., Martinsson, B., Orsini, D., Svenningsson, B., Swietlicki, E., Wiedensohler, A., Noone, K. J., Pahl, S., Winkler, P., Seyffer, E., Helas, G., Jaeschke, W., Georgii, H. W., Wobrock, W., Preiss, M., Maser, R., Schell, D., Dollard, G., Jones, B., Davies, T., Sedlak, D. L., David, M. M., Wendisch, M., Cape, J. N., Hargreaves, K. J., Sutton, M. A., StoretonWest, R. L., Fowler, D., Hallberg, A., Harrison, R. M., and Peak, J. D.: The Great Dun Fell Cloud Experiment 1993: An overview, Atmospheric Environment, 31, 2393-2405, 10.1016/s1352-2310(96)00316-0, 1997.

Croft, B., Lohmann, U., Martin, R. V., Stier, P., Wurzler, S., Feichter, J., Hoose, C., Heikkila, U., van Donkelaar, A., and Ferrachat, S.: Influences of in-cloud aerosol scavenging parameterizations on aerosol concentrations and wet deposition in ECHAM5-HAM, Atmos. Chem. Phys., 10, 1511-1543, 10.5194/acp-10-1511-2010, 2010.

Cross, E. S., Slowik, J. G., Davidovits, P., Allan, J. D., Worsnop, D. R., Jayne, J. T., Lewis †, D. K., Canagaratna, M., and Onasch, T. B.: Laboratory and Ambient Particle Density Determinations using Light Scattering in Conjunction with Aerosol Mass Spectrometry, Aerosol Sci. Technol., 41, 343-359, 10.1080/02786820701199736, 2007.

Demoz, B. B., Collett, J. L., and Daube, B. C.: On the Caltech Active Strand Cloudwater Collectors, Atmos. Res., 41, 47-62, 10.1016/0169-8095(95)00044-5, 1996.

Deng, Z., Zhao, C., Zhang, Q., Huang, M., and Ma, X.: Statistical analysis of microphysical properties and the parameterization of effective radius of warm clouds in Beijing area, Atmos. Res., 93, 888-896, 2009.

Drewnick, F., Schneider, J., Hings, S. S., Hock, N., Noone, K., Targino, A., Weimer, S., and Borrmann, S.: Measurement of ambient, interstitial, and residual aerosol particles on a mountaintop site in central Sweden using an aerosol mass spectrometer and a CVI, Journal of Atmospheric Chemistry, 56, 1-20, 10.1007/s10874-006-9036-8, 2007.

Durkee, P. A., Noone, K. J., Ferek, R. J., Johnson, D. W., Taylor, J. P., Garrett, T. J., Hobbs, P. V., Hudson, J. G., Bretherton, C. S., Innis, G., Frick, G. M., Hoppel, W. A., O'Dowd, C. D., Russell, L. M., Gasparovic, R., Nielsen, K. E., Tessmer, S. A., Ostrom, E., Osborne, S. R., Flagan, R. C., Seinfeld, J. H., and Rand, H.: The impact of ship-produced aerosols on the microstructure and albedo of warm marine stratocumulus clouds: A test of MAST hypotheses 1i and 1ii, Journal of the Atmospheric Sciences, 57, 2554-2569, 10.1175/1520-0469(2000)057<2554:Tiospa>2.0.Co;2, 2000.

Dusek, U., Frank, G. P., Hildebrandt, L., Curtius, J., Schneider, J., Walter, S., Chand, D., Drewnick, F., Hings, S., Jung, D., Borrmann, S., and Andreae, M. O.: Size matters more than chemistry for cloud-nucleating ability of aerosol particles, Science, 312, 1375-1378, 10.1126/science.1125261, 2006.

Ekman, A. M. L., Engstrom, A., and Soderberg, A.: Impact of Two-Way Aerosol-Cloud Interaction and Changes in Aerosol Size Distribution on Simulated Aerosol-Induced Deep Convective Cloud Sensitivity, J. Atmos. Sci., 68, 685-698, 10.1175/2010jas3651.1, 2011.

Fan, J., Leung, L. R., Rosenfeld, D., Chen, Q., Li, Z., Zhang, J., and Yan, H.: Microphysical effects determine macrophysical response for aerosol impacts on deep convective clouds, Proc. Natl. Acad. Sci. U. S. A., 110, E4581-E4590, 10.1073/pnas.1316830110, 2013.

Fan, J., Wang, Y., Rosenfeld, D., and Liu, X.: Review of Aerosol-Cloud Interactions: Mechanisms, Significance, and Challenges, J. Atmos. Sci., 73, 4221-4252, 10.1175/jas-d-16-0037.1, 2016.

Feingold, G., Remer, L. A., Ramaprasad, J., and Kaufman, Y. J.: Analysis of smoke impact on clouds in Brazilian biomass burning regions: An extension of Twomey's approach, J. Geophys. Res.: Atmos., 106, 22907-22922, 10.1029/2001jd000732, 2001.

Feingold, G.: Modeling of the first indirect effect: Analysis of measurement requirements, Geophys. Res. Lett., 30, 10.1029/2003gl017967, 2003.

Freud, E., and Rosenfeld, D.: Linear relation between convective cloud drop number concentration and depth for rain initiation, J. Geophys. Res.: Atmos., 117, 13, 10.1029/2011jd016457, 2012.

Frey, L., Bender, F. A. M., and Svensson, G.: Cloud albedo changes in response to anthropogenic sulfate and non-sulfate aerosol forcings in CMIP5 models, Atmos. Chem. Phys., 17, 9145-9162, 10.5194/acp-17-9145-2017, 2017.

Georgakakos, K. P., and Bras, R. L.: A hydrologically useful station precipitation model. I. Formulation, Water Resources Research, 20, 1585-1596, 10.1029/WR020i011p01585, 1984.

Grabowski, W. W., and Wang, L.-P.: Growth of Cloud Droplets in a Turbulent Environment, Annu. Rev. Fluid Mech., 45, 293-324, 10.1146/annurev-fluid-011212-140750, 2013.

Grandey, B. S., and Stier, P.: A critical look at spatial scale choices in satellite-based aerosol indirect effect studies, Atmos. Chem. Phys., 10, 11459-11470, 10.5194/acp-10-11459-2010, 2010.

Guo, J., Wang, Y., Shen, X. H., Wang, Z., Lee, T., Wang, X. F., Li, P. H., Sun, M. H., Collett, J. L., Wang, W. X., and Wang, T.: Characterization of cloud water chemistry at Mount Tai, China: Seasonal variation, anthropogenic impact, and cloud processing, Atmospheric Environment, 60, 467-476, 10.1016/j.atmosenv.2012.07.016, 2012.

Heikenfeld, M., White, B., Labbouz, L., and Stier, P.: Aerosol effects on deep convection: the propagation of aerosol perturbations through convective cloud microphysics, Atmos. Chem. Phys., 19, 2601-2627, 10.5194/acp-19-2601-2019, 2019.

Heintzenberg, J., Ogren, J. A., Noone, K. J., and Gardneus, L.: The Size Distribution of Submicrometer Particles within and about Stratocumulus Cloud Droplets on Mt. Areskutan, Sweden, Atmospheric Research, 24, 89-101, 10.1016/0169-8095(89)90039-2, 1989.

Hudson, J. G.: Variability of the relationship between particle size and cloud-nucleating ability, Geophys. Res. Lett., 34, 10.1029/2006gl028850, 2007.

Khain, A. P., Beheng, K. D., Heymsfield, A., Korolev, A., Krichak, S. O., Levin, Z., Pinsky, M., Phillips, V., Prabhakaran, T., Teller, A., van den Heever, S. C., and Yano, J. I.: Representation of microphysical processes in cloud-resolving models: Spectral (bin) microphysics versus bulk parameterization, Rev. Geophys., 53, 247-322, 10.1002/2014rg000468, 2015.

Koren, I., Kaufman, Y. J., Rosenfeld, D., Remer, L. A., and Rudich, Y.: Aerosol invigoration and restructuring of Atlantic convective clouds, Geophys. Res. Lett., 32, 10.1029/2005gl023187, 2005.

Lacis, A. A., and Hansen, J. E.: Parameterization for absorption of solar-radiation in earths atmosphere J. Atmos. Sci., 31, 118-133, 10.1175/1520-0469(1974)031<0118:Apftao>2.0.Co;2, 1974.

Li, J., Wang, X., Chen, J., Chao, Z., and Herrmann, H.: Chemical composition and droplet size distribution of cloud at the summit of Mount Tai, China, Atmos. Chem. Phys., 17, 1-21, 2017a.

Li, P., Li, X., Yang, C., Wang, X., Chen, J., and Jr, J. L. C.: Fog water chemistry in Shanghai, Atmos. Environ., 45, 4034-4041,

2011.
Li, S., Joseph, E., Min, Q., and Yin, B.: Multi-year ground-based observations of aerosol-cloud interactions in the Mid-Atlantic of the United States, J. Quant. Spectrosc. Radiat. Transfer, 188, 192-199, 10.1016/j.jqsrt.2016.02.004, 2017b.
Lohmann, U., and Feichter, J.: Global indirect aerosol effects: a review, Atmos. Chem. Phys., 5, 715-737, 10.5194/acp-5-715-2005, 2005.
Lu, C., Niu, S., Tang, L., Lv, J., Zhao, L., and Zhu, B.: Chemical composition of fog water in Nanjing area of China and its related fog microphysics, Atmos. Res., 97, 47-69, 2010.
Lu, M.-L., Conant, W. C., Jonsson, H. H., Varutbangkul, V., Flagan, R. C., and Seinfeld, J. H.: The Marine Stratus/Stratocumulus Experiment (MASE): Aerosol-cloud relationships in marine stratocumulus, J. Geophys. Res.: Atmos., 112, 10.1029/2006jd007985, 2007.
Mazoyer, M., Burnet, F., Denjean, C., Roberts, G. C., Haeffelin, M., Dupont, J. C., and Elias, T.: Experimental study of the aerosol impact on fog microphysics, Atmos. Chem. Phys., 19, 4323-4344, 10.5194/acp-19-4323-2019, 2019.
McComiskey, A., Feingold, G., Frisch, A. S., Turner, D. D., Miller, M. A., Chiu, J. C., Min, Q., and Ogren, J. A.: An assessment of aerosol-cloud interactions in marine stratus clouds based on surface remote sensing, J. Geophys. Res.: Atmos., 114, -, 2009.
McFiggans, G., Artaxo, P., Baltensperger, U., Coe, H., Facchini, M. C., Feingold, G., Fuzzi, S., Gysel, M., Laaksonen, A., Lohmann, U., Mentel, T. F., Murphy, D. M., O'Dowd, C. D., Snider, J. R., and Weingartner, E.: The effect of physical and chemical aerosol properties on warm cloud droplet activation, Atmos. Chem. Phys., 6, 2593-2649, 10.5194/acp-6-2593-2006, 2006.
Mertes, S., Galgon, D., Schwirn, K., Nowak, A., Lehmann, K., Massling, A., Wiedensohler, A., and Wieprecht, W.: Evolution of particle concentration and size distribution observed upwind, inside and downwind hill cap clouds at connected flow conditions during FEBUKO, Atmos. Environ., 39, 4233-4245, 10.1016/j.atmosenv.2005.02.009, 2005.
Modini, R. L., Frossard, A. A., Ahlm, L., Russell, L. M., Corrigan, C. E., Roberts, G. C., Hawkins, L. N., Schroder, J. C., Bertram, A. K., Zhao, R., Lee, A. K. Y., Abbatt, J. P. D., Lin, J., Nenes, A., Wang, Z., Wonaschuetz, A., Sorooshian, A., Noone, K. J., Jonsson, H., Seinfeld, J. H., Toom-Sauntry, D., Macdonald, A. M., and Leaitch, W. R.: Primary marine aerosol-cloud interactions off the coast of California, Journal of Geophysical Research-Atmospheres, 120, 4282-4303, 10.1002/2014jd022963, 2015.
Möller, D., Acker, K., and Wieprecht, W.: A relationship between liquid water content and chemical composition in clouds, Atmos. Res., 41, 321-335, 1996.
Noone, K. J., Ogren, J. A., and Heintzenberg, J.: An Examination of Clouds at a Mountain-Top Site in Central Sweden: The Distribution of Solute within Cloud Droplets, Atmospheric Research, 25, 3-15, 10.1016/0169-8095(90)90002-t, 1990.
Padmakumari, B., Maheskumar, R. S., Anand, V., and Axisa, D.: Microphysical characteristics of convective clouds over ocean and land from aircraft observations, Atmos. Res., 195, 62-71, 10.1016/j.atmosres.2017.05.011, 2017.
Penner, J. E., Dong, X. Q., and Chen, Y.: Observational evidence of a change in radiative forcing due to the indirect aerosol effect, Nature, 427, 231-234, 10.1038/nature02234, 2004.
Platnick, S., Durkee, P. A., Nielsen, K., Taylor, J. P., Tsay, S. C., King, M. D., Ferek, R. J., Hobbs, P. V., and Rottman, J. W.: The role of background cloud microphysics in the radiative formation of ship tracks, Journal of the Atmospheric Sciences, 57, 2607-2624, 10.1175/1520-0469(2000)057<2607:Trobcm>2.0.Co;2, 2000.
Qian, Y., Gong, D. Y., Fan, J. W., Leung, L. R., Bennartz, R., Chen, D. L., and Wang, W. G.: Heavy pollution suppresses light rain in China: Observations and modeling, J. Geophys. Res.: Atmos., 114, 16, 10.1029/2008jd011575, 2009.
Quante, M.: The role of clouds in the climate system, J. Phys. IV, 121, 61-86, 10.1051/jp4:2004121003, 2004.
Reid, J. S., Hobbs, P. V., Rangno, A. L., and Hegg, D. A.: Relationships between cloud droplet effective radius, liquid water content, and droplet concentration for warm clouds in Brazil embedded in biomass smoke, J. Geophys. Res.: Atmos., 104, 6145-6153, 1999.
Rose, D., Gunthe, S. S., Mikhailov, E., Frank, G. P., Dusek, U., Andreae, M. O., and Poeschl, U.: Calibration and measurement uncertainties of a continuous-flow cloud condensation nuclei counter (DMT-CCNC): CCN activation of ammonium sulfate and sodium chloride aerosol particles in theory and experiment, Atmospheric Chemistry and Physics, 8, 1153-

1179, 10.5194/acp-8-1153-2008, 2008.
Rosenfeld, D.: Aerosol-cloud interactions control of earth radiation and latent heat release budgets, Space Sci. Rev., 125, 149-157, 10.1007/s11214-006-9053-6, 2006.
Rosenfeld, D., Andreae, M. O., Asmi, A., Chin, M., de Leeuw, G., Donovan, D. P., Kahn, R., Kinne, S., Kivekas, N., Kulmala, M., Lau, W., Schmidt, K. S., Suni, T., Wagner, T., Wild, M., and Quaas, J.: Global observations of aerosol-cloud-precipitation-climate interactions, Rev. Geophys., 52, 750-808, 10.1002/2013rg000441, 2014a.
Rosenfeld, D., Sherwood, S., Wood, R., and Donner, L.: Climate Effects of Aerosol-Cloud Interactions, Science, 343, 379-380, 10.1126/science.1247490, 2014b.
Roth, A., Schneider, J., Klimach, T., Mertes, S., van Pinxteren, D., Herrmann, H., and Borrmann, S.: Aerosol properties, source identification, and cloud processing in orographic clouds measured by single particle mass spectrometry on a central European mountain site during HCCT-2010, Atmos. Chem. Phys., 16, 505-524, 10.5194/acp-16-505-2016, 2016.
Sant, V., Lohmann, U., and Seifert, A.: Performance of a Triclass Parameterization for the Collision-Coalescence Process in Shallow Clouds, J. Atmos. Sci., 70, 1744-1767, 10.1175/jas-d-12-0154.1, 2013.
Schroder, J. C., Hanna, S. J., Modini, R. L., Corrigan, A. L., Kreidenweis, S. M., Macdonald, A. M., Noone, K. J., Russell, L. M., Leaitch, W. R., and Bertram, A. K.: Size-resolved observations of refractory black carbon particles in cloud droplets at a marine boundary layer site, Atmospheric Chemistry and Physics, 15, 1367-1383, 10.5194/acp-15-1367-2015, 2015.
Seinfeld, J. H., and Pandis, S. N.: Atmospheric Chemistry and Physics: From Air Pollution to Climate Change, John Wiley & Sons, Inc., Hoboken, New Jersey, 2006.
Seinfeld, J. H., Bretherton, C., Carslaw, K. S., Coe, H., DeMott, P. J., Dunlea, E. J., Feingold, G., Ghan, S., Guenther, A. B., Kahn, R., Kraucunas, I., Kreidenweis, S. M., Molina, M. J., Nenes, A., Penner, J. E., Prather, K. A., Ramanathan, V., Ramaswamy, V., Rasch, P. J., Ravishankara, A. R., Rosenfeld, D., Stephens, G., and Wood, R.: Improving our fundamental understanding of the role of aerosol-cloud interactions in the climate system, Proc. Natl. Acad. Sci. U. S. A., 113, 5781-5790, 2016.
Shen, L., Wang, H., Yin, Y., Chen, J., and Chen, K.: Observation of atmospheric new particle growth events at the summit of mountain Tai (1534 m) in Central East China, Atmos. Environ., 201, 148-157, 10.1016/j.atmosenv.2018.12.051, 2019.
Spiegel, J. K., Zieger, P., Bukowiecki, N., Hammer, E., Weingartner, E., and Eugster, W.: Evaluating the capabilities and uncertainties of droplet measurements for the fog droplet spectrometer (FM-100), Atmospheric Measurement Techniques, 5, 2237-2260, 10.5194/amt-5-2237-2012, 2012.
Stephens, G. L.: Radiation profiles in extended water clouds. II. Parameterization schemes, Journal of the Atmospheric Sciences, 35, 2123-2132, 10.1175/1520-0469(1978)035<2123:Rpiewc>2.0.Co;2, 1978.
Stevens, B., and Bony, S.: What Are Climate Models Missing?, Science, 340, 1053-1054, 10.1126/science.1237554, 2013.
Tang, J. P., Wang, P. C., Mickley, L. J., Xia, X. G., Liao, H., Yue, X., Sun, L., and Xia, J. R.: Positive relationship between liquid cloud droplet effective radius and aerosol optical depth over Eastern China from satellite data, Atmos. Environ., 84, 244-253, 10.1016/j.atmosenv.2013.08.024, 2014.
Targino, A. C., Noone, K. J., Drewnick, F., Schneider, J., Krejci, R., Olivares, G., Hings, S., and Borrmann, S.: Microphysical and chemical characteristics of cloud droplet residuals and interstitial particles in continental stratocumulus clouds, Atmospheric Research, 86, 225-240, 10.1016/j.atmosres.2007.05.001, 2007.
Twohy, C. H., Petters, M. D., Snider, J. R., Stevens, B., Tahnk, W., Wetzel, M., Russell, L., and Burnet, F.: Evaluation of the aerosol indirect effect in marine stratocumulus clouds: Droplet number, size, liquid water path, and radiative impact, J. Geophys. Res.: Atmos., 110, -, 2005.
Twomey, S.: Pollution and planetary albedo, Atmos. Environ., 8, 1251-1256, 10.1016/0004-6981(74)90004-3, 1974.
Twomey, S. A.: The Influence of Pollution on the Shortwave Albedo of Clouds, J. Atmos. Sci., 34, 1149-1154, 1977.
Van Pinxteren, D., Fomba, K. W., Mertes, S., Müller, K., Spindler, G., Schneider, J., Lee, T., Collett, J. L., and Herrmann, H.: Cloud water composition during HCCT-2010: Scavenging efficiencies, solute concentrations, and droplet size dependence of inorganic ions and dissolved organic carbon, Atmos. Chem. Phys., 15, 24311-24368, 2016.
Verheggen, B., Cozic, J., Weingartner, E., Bower, K., Mertes, S., Connolly, P., Gallagher, M., Flynn, M., Choularton, T., and Baltensperger, U.: Aerosol partitioning between the interstitial and the condensed phase in mixed-phase clouds, Journal

of Geophysical Research-Atmospheres, 112, 13, 10.1029/2007jd008714, 2007.
Wang, F., Guo, J., Wu, Y., Zhang, X., Deng, M., Li, X., Zhang, J., and Zhao, J.: Satellite observed aerosol-induced variability in warm cloud properties under different meteorological conditions over eastern China, Atmos. Environ., 84, 122-132, 10.1016/j.atmosenv.2013.11.018, 2014.
Wang, Y., Guo, J., Wang, T., Ding, A., Gao, J., Yang, Z., Jr, J. L. C., and Wang, W.: Influence of regional pollution and sandstorms on the chemical composition of cloud/fog at the summit of Mt. Taishan in northern China, Atmos. Res., 99, 434-442, 2011.
Welch, R. M., Asefi, S., Zeng, J., Nair, U. S., Han, Q., Lawton, R. O., Ray, D. K., and Manoharan, V. S.: Biogeography of tropical montane cloud forests. Part I: Remote sensing of cloud-base heights, Journal of Applied Meteorology and Climatology, 47, 960-975, 10.1175/2007jamc1668.1, 2008.
Yuan, T., Li, Z., Zhang, R., and Fan, J.: Increase of cloud droplet size with aerosol optical depth: An observation and modeling study, J. Geophys. Res.: Atmos., 113, 10.1029/2007jd008632, 2008.
Zhang, L. M., Michelangeli, D. V., and Taylor, P. A.: Numerical studies of aerosol scavenging by low-level, warm stratiform clouds and precipitation, Atmos. Environ., 38, 4653-4665, 10.1016/j.atmosenv.2004.05.042, 2004a.
Zhang, X., Musson-Genon, L., Dupont, E., Milliez, M., and Carissimo, B.: On the Influence of a Simple Microphysics Parametrization on Radiation Fog Modelling: A Case Study During ParisFog, Boundary-Layer Meteorol., 151, 293-315, 10.1007/s10546-013-9894-y, 2014.
Zhang, Y., Rossow, W. B., Lacis, A. A., Oinas, V., and Mishchenko, M. I.: Calculation of radiative fluxes from the surface to top of atmosphere based on ISCCP and other global data sets: Refinements of the radiative transfer model and the input data, J. Geophys. Res.: Atmos., 109, 10.1029/2003JD004457 J. Geophys. Res. 2018/12/31 doi: 10.1029/2003JD004457, 2004b.
Zhao, C., Klein, S. A., Xie, S., Liu, X., Boyle, J. S., and Zhang, Y.: Aerosol First Indirect Effects on Non-Precipitating Low-Level Liquid Cloud Properties as Simulated by CAM5 at ARM Sites, AGU Fall Meeting, 2012, 376-395,
Zhao, C., Qiu, Y., Dong, X., Wang, Z., Peng, Y., Li, B., Wu, Z., and Wang, Y.: Negative Aerosol-Cloud re Relationship from Aircraft Observations over Hebei, China, Earth Space Sci., 5, 2018.
Zhou, Y., Wang, T., Gao, X., Xue, L., Wang, X., Wang, Z., Gao, J., Zhang, Q., and Wang, W.: Continuous observations of water-soluble ions in PM 2.5 at Mount Tai (1534 m a.s.l.) in central-eastern China, J. Atmos. Chem., 64, 107-127, 2009.
Zhu, C., Chen, J., Wang, X., Li, J., Wei, M., Xu, C., Xu, X., Ding, A., and Collett, J. L., Jr.: Chemical Composition and Bacterial Community in Size-Resolved Cloud Water at the Summit of Mt. Tai, China, Aerosol Air Qual. Res., 18, 1-14, 10.4209/aaqr.2016.11.0493, 2018.

Tables and Figures

Table 1: Comparison of clouds monitored at Mt. Tai with city fogs, convective clouds monitored by research aircrafts and other orographic clouds. Including sampling information (site, period and altitude), the range of $PM_{2.5}$ mass concentrations, the range of microphysical parameters (number concentrations of cloud droplets-N_C, liquid water content-*LWC*, median volume diameter- *MVD*, effective radius-r_{eff}) and the number of monitored clouds/cloud events/fog events.

Sampling Site	Period	Altitude (m a.s.l)	$PM_{2.5}$ ($\mu g\ m^{-3}$)	N_C ($\#\ cm^{-3}$)	*LWC* ($g\ m^{-3}$)	*MVD* (μm)	r_{eff} (μm)	Number of clouds/cloud events/fog events	Reference
City Fog									
Shanghai, China	Nov. 2009	7	-	11-565	0.01-0.14	5.0-20.0	-	1	(Li et al., 2011)
Nanjing, China	Dec. 2006- Dec. 2007	22	0.03[a]-0.60[a]	-	2.69e^{-3}-0.16	-	1.6[b]-2.7[b]	7	(Lu et al., 2010)
Convective Clouds									
Amazon Basin/cerrado reCompagions, Brazil	Aug.-Sept. 1995	90-4000	-	-	0[d]-2.10[d]	-	2.8[d]-9.2[d]	>1000	(Reid et al., 1999)
Hyderabad - The Bay of Bengal, India	29th Oct. 2010	1300-6300		10[d]-380	0[d]-1.80		3.8[d]-17.0	1	(Padmakumari et al., 2017)
Orographic clouds									
Mt. Schmücke, Germany	Sep.-Oct. 2010	937	-	-	0.14-0.37	-	5.7-8.7	8	(Van Pinxteren et al., 2016)
East Peak Mountain, Puerto Rico	Dec. 2004	1040	-	193-519	0.24-0.31	14.0-20.0	-	2	(Allan et al., 2008)
Mt. Tai, China	Jul.-Aug. 2014	1545	11.1-173.3	4-2186	0.01-1.52	1.6-43.0	0.8-18.9	24	Unpublished data from (Li et al., 2017a)
Mt. Tai, China	Jun.-Jul. 2018	1545	1.2-127.1	10-3163	1.01e^{-3}-1.47	4.4-25.0	2.4-13.4	40	This study
Mt. Tai, China (CP-1[c])	10th – 13th Jul. 2018	1545	1.3-40.7	11-2470	1.12e^{-3}-1.47	4.6-17.4	2.5-10.7	12	This study
Mt. Tai, China (CP-2[c])	13th – 20th Jul. 2018	1545	1.2-66.2	10-3163	1.03e^{-3}-1.10	4.6-13.5	2.4-7.9	12	This study

[a] Represents the mass concentrations of PM_{10}.. [b] Represents the range of averaged radium. [c] Two cloud processes which are detailedly discussed in this study. [d] Values were read from the graphs.

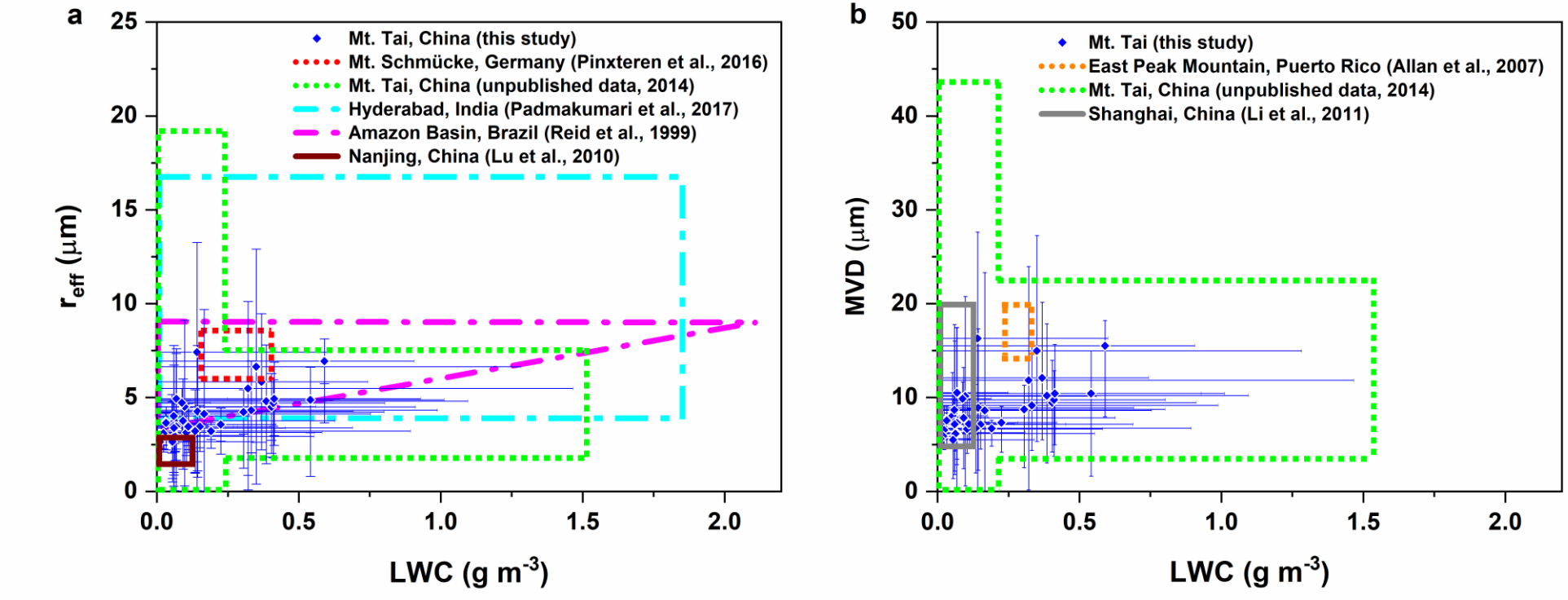

Figure 1: Plots of effective radius (r_{eff}, a) or medium volume diameter (*MVD*, b) against liquid water content (*LWC*) for clouds and fogs from the literatures. "……", "– · –" and "——" represents orographic clouds, convective clouds and city fogs, respectively. The areas represented the range of data obtained from the corresponding observations. The blue diamonds with error bars represented the average *LWC* and r_{eff} (or *MVD*) of 40 cloud events observed at Mt. Tai in the present study with corresponding ranges.

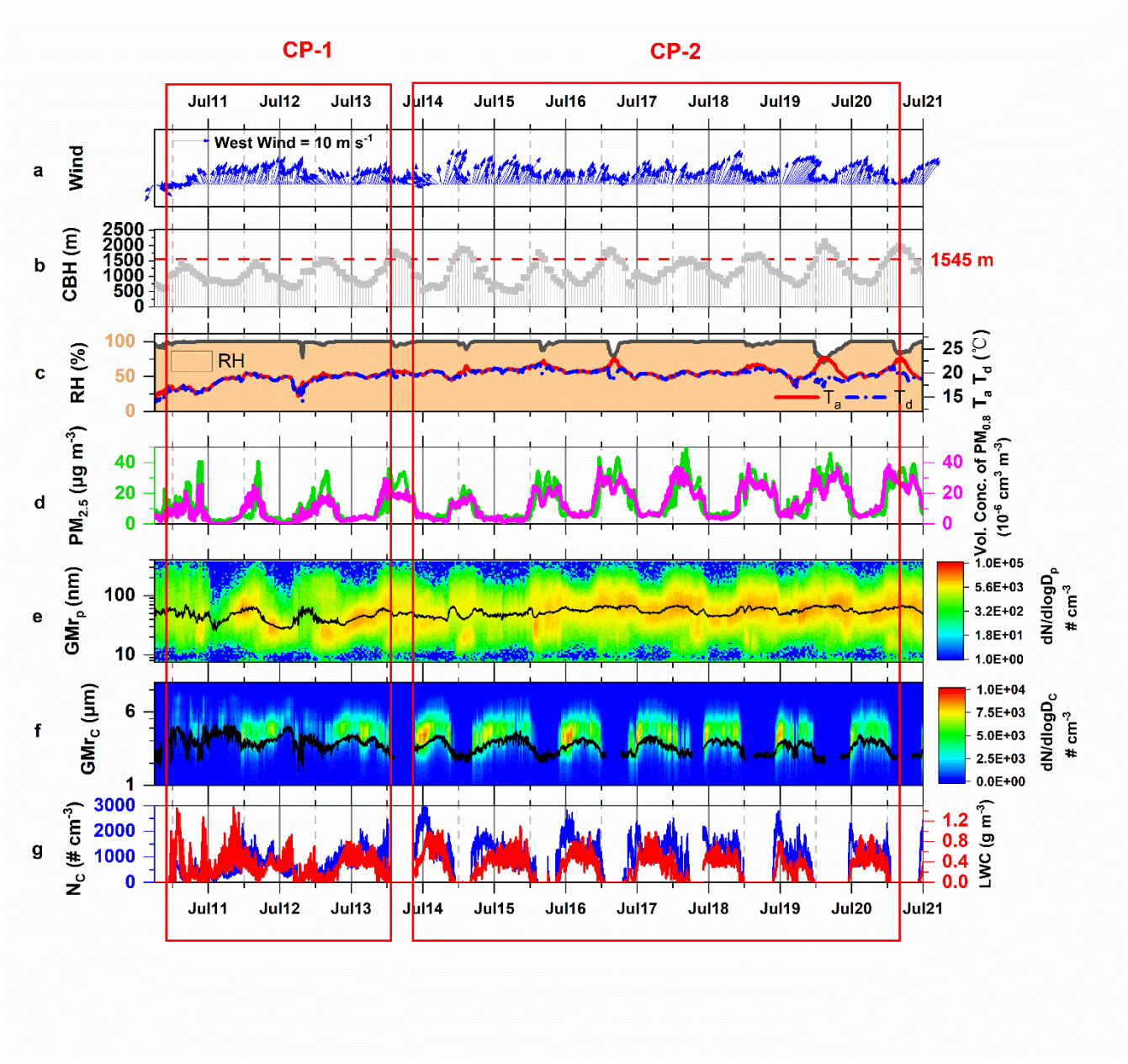

Figure 2: The monitoring information of CP-1 and CP-2. Including (a) Wind speed (*WS*, m s^{-1}) and wind direction (*WD*), (b) cloud based height (*CBH*, m) (c)relative humidity (*RH*, %), ambient temperature (T_a, ℃) and dew point temperature (T_d, ℃) (d) $PM_{2.5}$ mass concentrations (μg m^{-3}) and volumn concentration of $PM_{0.8}$ (10^{-6} cm^3 cm^{-3}) (e) size distribution of particles (13.6-763.5 nm) and corresponding geometric mean radius (GMr_P) (f) size distribution of cloud droplets (2-50 μm) and corresponding geometric mean radius (GMr_C) (g) N_C and *LWC* of cloud droplets.

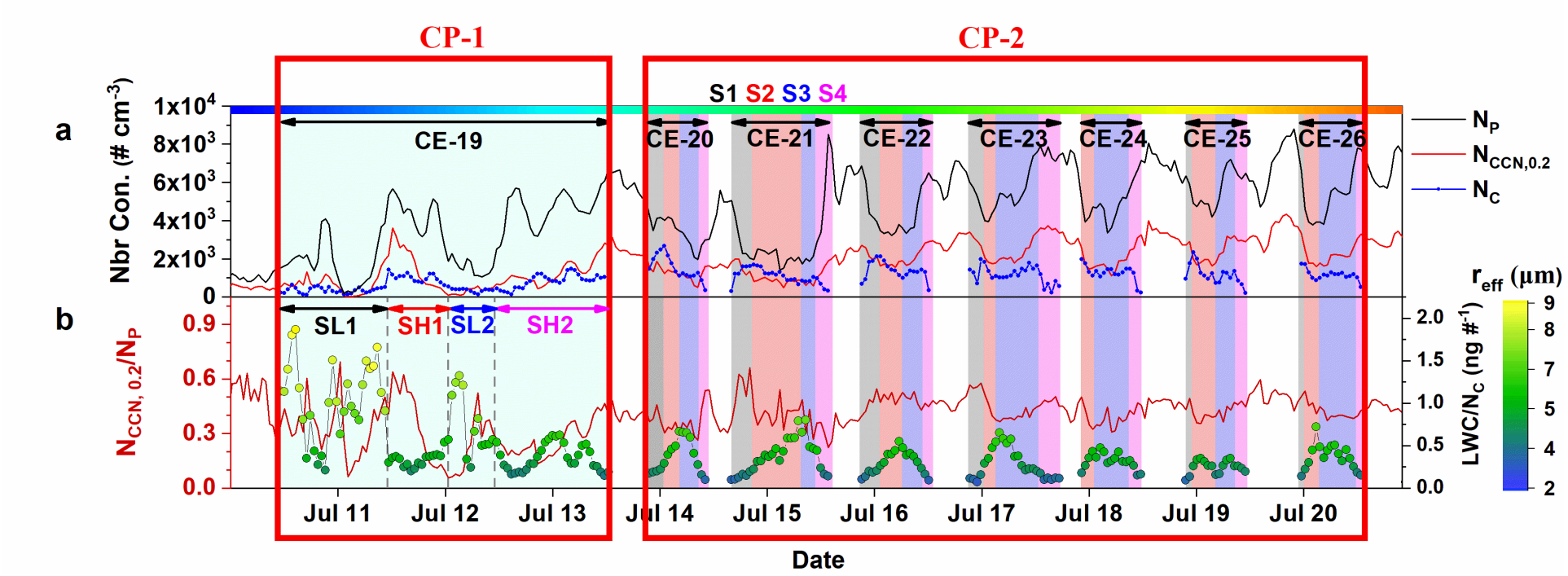

Figure 3: Variation of (a) N_C, N_p and $N_{CCN,0.2}$ (b) $N_{CCN,0.2}/N_P$ and LWC/N_C during CP-1 and CP-2.

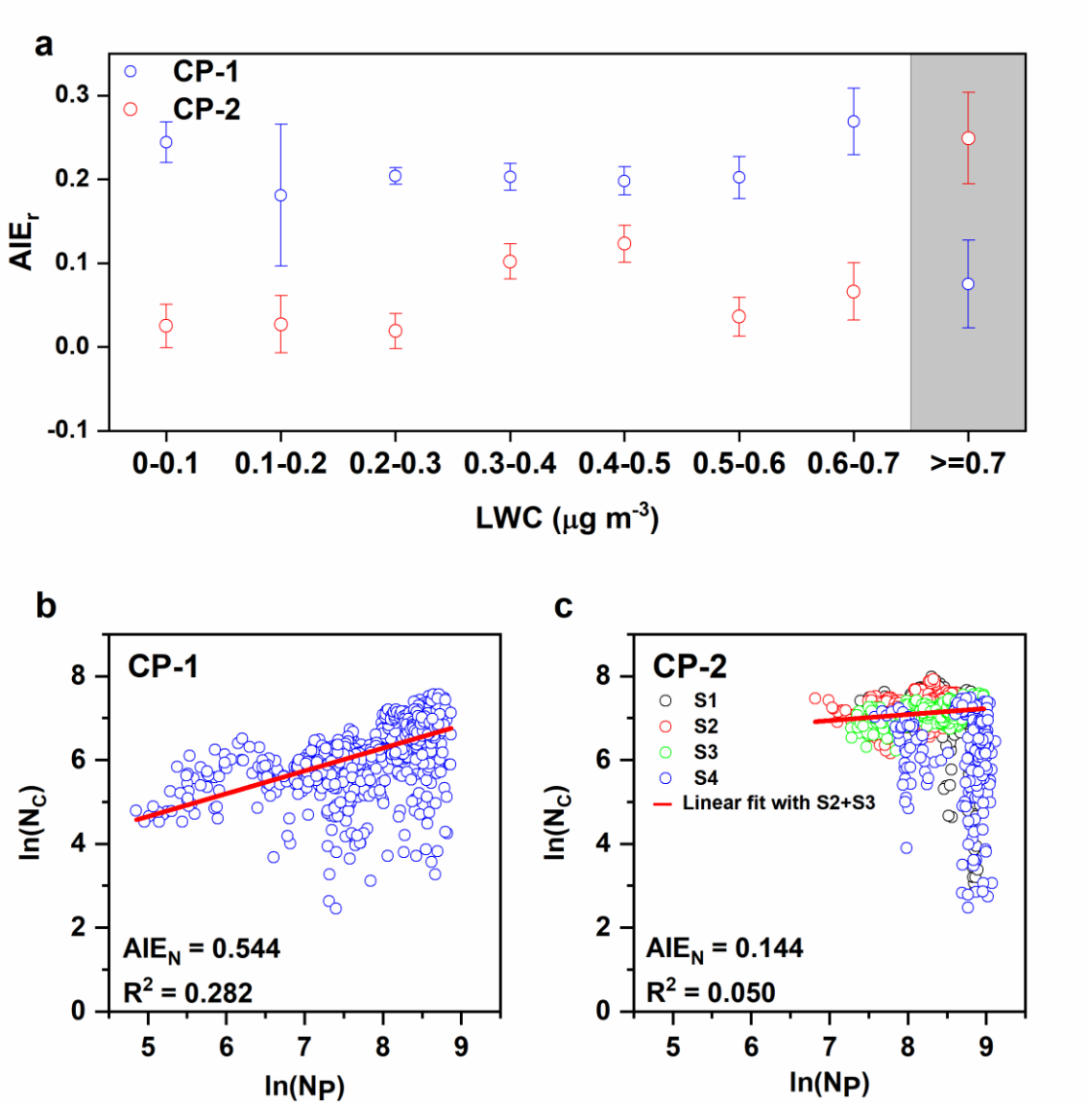

Figure 4: (a) The determination of AIE_r for each LWC bin with 0.1 g m^{-3}. The determination of AIE_N based on N_C (b) during CP-1 and (c) during CP-2.

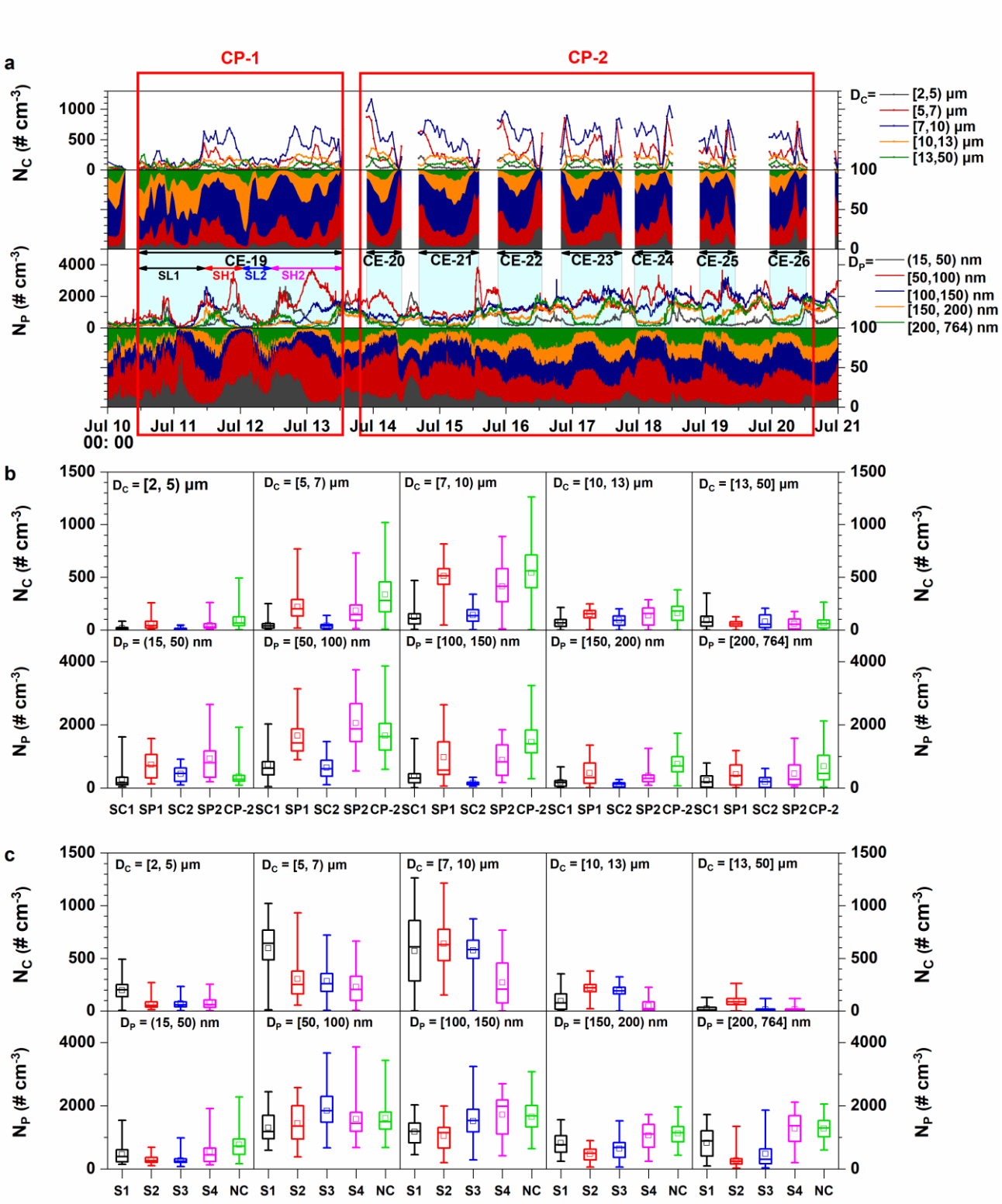

Figure 5: Size distribution of particles and cloud droplets during CP-1 and CP-2. (a) Time series plot of N_C in five size ranges ([2, 5) µm, [5, 7) µm, [7, 10) µm, [10, 13) µm and [13, 50) µm) and N_P in five size ranges ((15, 50) nm, [50, 100) nm, [100, 150) nm, [150, 200) nm, [200, 765) nm). (b) five size ranges of N_C and five size ranges of N_P in SL1, SH1, SL2, SH2 and CP-2 (c) five size ranges of N_C and five size ranges of N_P in S1, S2, S3 ,S4 and NC ("NC" in (c) represents particle size distributions during cloudless period).

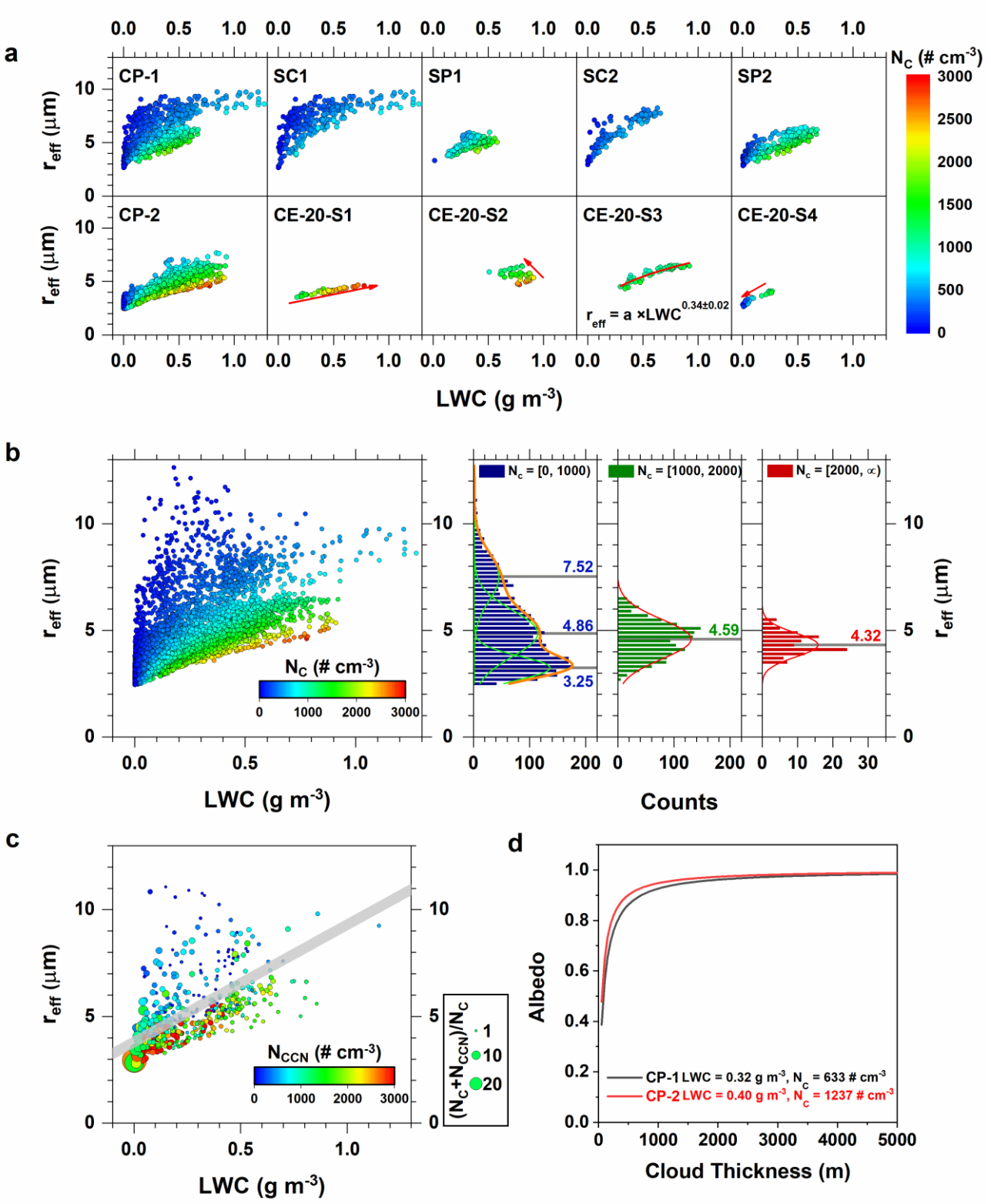

Figure 6: The plot of *LWC* versus r_{eff} (a) in different cloud stages of CP-1 and CP-2 (b) under different N_C ranges (c) under different N_{CCN}. The time resolution of the corresponding data was 5 min in (a), (b) and 50 min in (c). (d) The plot of albedo versus the variation of cloud thickness during CP-1 and CP-2. The averaged values of *LWC* and N_C of CP-1 and CP-2 were applied to calculate albedo according to the equations in Section 2.8.